5-2019

Parameterizing Wave-Driven Vertical Constituent Transport in the Upper Atmosphere

Chester S. Gardner

Yafang Guo
University of North Dakota, yafang.guo@UND.edu

Alan Z. Liu

Earth and Space Science

RESEARCH ARTICLE
10.1029/2019EA000625

Parameterizing Wave-Driven Vertical Constituent Transport in the Upper Atmosphere

Chester S. Gardner[1], **Yafang Guo**[2], **and Alan Z. Liu**[3]

[1]Department of Electrical and Computer Engineering, University of Illinois at Urbana-Champaign, Urbana, IL, USA, [2]Department of Atmospheric Sciences, University of North Dakota, Grand Forks, ND, USA, [3]Center for Space and Atmospheric Research, Department of Physical Sciences, Embry-Riddle Aeronautical University, Daytona Beach, FL, USA

Key Points:
- Dissipating waves induce strong vertical transport of atmospheric species, which has not been fully incorporated in global models
- Wave-driven constituent transport can be predicted in terms of quantities that are readily derived from many wave parameterization schemes
- Transport predictions compare favorably with observations of the mesopause region at midlatitudes

Supporting Information:
- Supporting Information S1

Correspondence to:
C. S. Gardner,
cgardner@illinois.edu

Citation:
Gardner, C. S., Guo, Y., & Liu, A. Z. (2019). Parameterizing wave-driven vertical constituent transport in the upper atmosphere. *Earth and Space Science*, *6*. https://doi.org/10.1029/2019EA000625

Received 16 MAR 2019
Accepted 30 APR 2019
Accepted article online 14 MAY 2019

Abstract Dissipating waves contribute to vertical mixing of the atmosphere, alter molecular and eddy diffusion, and induce chemical transport of reactive species. These processes induce strong vertical transport of atmospheric constituents in regions where wave dissipation is significant. The effective wave diffusivity is proportional to the Stokes drift velocity imparted by the spectrum of vertically propagating waves, which is related to the vertical heat and wave energy fluxes. Because the heat flux cannot be derived from wave parameterization schemes employed in most atmospheric models, wave-driven constituent transport has not been fully incorporated. However, we show in this paper that wave diffusivity can also be expressed in terms of the eddy diffusivity and variances of the temperature and lapse rate fluctuations, quantities that are readily derived from many wave parameterizations. The theory is in good agreement with lidar measurements of heat fluxes in the mesopause region. Total dynamical diffusivity associated with dissipating waves and turbulence can exceed 300 m^2/s near the mesopause.

1. Introduction

Gravity waves play important roles in the vertical transport of heat and atmospheric constituents, especially in the upper atmosphere where wave amplitudes are large and dissipation is significant (Gardner & Liu, 2010; Liu & Gardner, 2004; Walterscheid, 1981; Walterscheid & Schubert, 1989; Xu et al., 2003; Zhu et al., 2010). For example, waves help transport atomic oxygen, the meteoric metals, and nitric oxide from the upper atmosphere through the mesopause region into the lower atmosphere where these species, and the compounds they form, impact atmospheric chemistry and cloud formation (e.g., Crutzen, 1970; Lary, 1997; Plane, 2012; Plane et al., 2015; Shepherd et al., 2004; Smith et al., 2010; Ward, 1999). Most global atmospheric models cannot resolve the important smaller-scale waves, so wave transport processes are usually incorporated simply by considering the eddy diffusion generated when waves break (Garcia et al., 2014; Garcia & Solomon, 1985, 1994; Marsh et al., 2007). However, wave-induced dynamical and chemical transport processes also play important roles so that this simplified approach is not entirely adequate, as has been shown when modeling the mesospheric Na and Fe layers (Carrillo-Sánchez et al., 2016; Feng et al., 2013; Gardner et al., 2016; Marsh et al., 2013).

Dissipating waves induce strong vertical mixing, alter molecular and eddy diffusion, and induce chemical transport of reactive species. Several early attempts to account for enhanced wave transport in global models employed the concept of an effective wave diffusivity that is proportional to the eddy diffusivity (Grygalashvyly et al., 2012; Nakamura, 2001; Winters & D'Asaro, 1996). In this formulation, the dissipating waves enhance the down gradient eddy mixing. Recently, it was shown that the wave diffusivity is related to the vertical heat flux and is much larger than predicted by earlier studies (Gardner, 2018). Because waves induce pressure fluctuations, the diffusivity can also be expressed in terms of the vertical fluxes of wave energy and potential temperature. Unfortunately, existing wave parameterization schemes that are employed in most atmospheric models cannot be used to compute the heat and potential temperature fluxes. Therefore, it has not been possible to adapt this theory to the models.

Here, we extend our previous analyses by showing that the effective wave diffusivity is proportional to the Stokes drift velocity imparted by the vertically propagating waves, which can be expressed in terms of the eddy diffusivity and the variances of the wave-driven temperature and lapse rate fluctuations. These three parameters can be readily derived from most gravity wave parameterization schemes, and so it should

now be possible to fully account for wave-induced constituent transport (including chemical transport) in the global models. The theory is shown to be in sensible agreement with extensive mesopause region observations of winds and temperatures at the Starfire Optical Range (SOR), NM, and Cerro Pachón (CP), Chile, where the vertical heat fluxes were also measured (Gardner & Liu, 2007; Guo et al., 2017).

2. Generalized Constituent Transport

The effective vertical transport velocity of a species is defined as its vertical flux divided by its mean density. When the chemical production of a species C is slow compared to the periods of the dominant gravity waves, its total vertical transport velocity ($\overline{w}_{\mathrm{Trans}}$), induced by molecular diffusion, eddy mixing and wave effects, is given by (Gardner, 2018; Gardner & Liu, 2016)

$$\overline{w}_{\mathrm{Trans}} = \frac{\overline{w'[M]'}}{[\overline{M}]} - \frac{[\overline{M}]}{[\overline{C}]}\frac{\partial}{\partial z}\left(\frac{[\overline{C}]}{[\overline{M}]}\right)K_{\mathrm{Tot}} + \overline{w}_{\mathrm{Chem}} \tag{1}$$

where

$$0 \le \frac{\overline{w'[M]'}}{[\overline{M}]} = \frac{\overline{w'p'}}{\overline{p}} - \frac{\overline{w'T'}}{\overline{T}} \quad , \tag{2}$$

$$K_{\mathrm{Tot}} = \left[1 + \frac{\overline{(\partial T'/\partial z)^2}}{(\Gamma_{\mathrm{ad}} + \partial\overline{T}/\partial z)^2}\right](K_{\mathrm{Mole}} + K_{zz}) + K_{\mathrm{Wave}} \quad , \tag{3}$$

and

$$\overline{w}_{\mathrm{Chem}} = \left[\frac{N^2}{g}(\omega_C\alpha_C - \omega_{\mu C}) + \left(\frac{\partial\overline{Q}_C/[\overline{C}]}{\partial z} - \frac{\mu_C}{[\overline{C}]^2}\frac{\partial[\overline{C}]}{\partial z}\right)\right]\frac{\overline{(T')^2}}{(\Gamma_{\mathrm{ad}} + \partial\overline{T}/\partial z)^2}. \tag{4}$$

where $[C]$ is the density of C, $[M]$ is the density of the background atmosphere, w is the vertical velocity, T is the temperature, p is the pressure, $\overline{w'[M]'/[M]}$ is the Stokes drift velocity of the atmosphere associated with vertically propagating waves (e.g., Coy et al., 1986), $\overline{w'T'}$ is the wave-induced heat flux, $\overline{w'p'}$ is the wave energy flux, $\Gamma_{\mathrm{ad}} = g/C_p$ is the adiabatic lapse rate, g = 9.5 m/s is the gravitational acceleration, C_p = 1,003 $\mathrm{m^2{\cdot}K^{-1}{\cdot}s^{-2}}$ is the specific heat at constant pressure, N is the buoyancy frequency and K_{Tot}, K_{Mole}, K_{zz}, and K_{Wave} are respectively, the total, molecular, eddy, and wave diffusivities. The over bar denotes the mean quantity and prime denotes the wave-perturbed quantity. The remaining parameters in (4) are related to species chemistry and are defined in Gardner (2018).

Because the wave energy flux is positive and the heat flux is generally negative for dissipating, upwardly propagating waves, Stokes drift induced by the waves transports the background atmosphere upward as shown by (2). Of course, to maintain continuity, there must be descent elsewhere (Coy et al., 1986). The wave-driven constituent perturbations enhance the molecular and eddy diffusivities by a factor that is proportional to the temperature lapse rate variance as shown in (3), while the random vertical displacement fluctuations, induced by the full spectrum of waves, contribute to vertical mixing of the atmosphere similar to turbulence. As will be shown below, the effective wave diffusivity is proportional to the vertical Stokes drift velocity. Finally, chemical transport arises when perturbations of the vertical winds are correlated with the fluctuations in C caused by perturbations in the chemistry of C. Waves perturb chemistry by perturbing the temperature dependent reaction rates and the densities of all the species involved in the reactions. When wave perturbations are neglected, which is equivalent to assuming that T', p', and w' are 0, (1) reduces to the classical formula where $K_{\mathrm{Tot}} = K_{\mathrm{Mole}} + K_{zz}$. In this special case, vertical transport is determined solely by molecular diffusion and eddy mixing.

The effective wave diffusivity is given by (Gardner, 2018)

$$K_{\mathrm{Wave}} = \overline{w'\zeta} \tag{5}$$

where ζ is related to the vertical displacement induced by the spectrum of waves and is a solution to

$$\frac{\partial \zeta}{\partial t} = w' - \underline{V}' \bullet \nabla \zeta. \tag{6}$$

$\underline{V}'$ is the perturbed velocity field (see below). In previous studies, Liu and Gardner (2004) and Gardner and Liu (2010, 2016) employed the first-order perturbation solution to (6) to calculate ζ and $\overline{w'\zeta}$. Here, we take an alternative approach by using a modified version of the exact solution to (6) for a monochromatic gravity wave that was derived by Gardner and Shelton (1985).

3. Deriving K_{Wave}

For a monochromatic gravity wave the perturbed velocity field $\underline{V}' = u'\hat{x} + w'\hat{z}$ is a traveling wave, which is a function of $\varphi(\omega t - \underline{k} \bullet \underline{r})$, where u' and w' are, respectively, the horizontal and vertical wind perturbations, ω is the intrinsic frequency of the wave, $\underline{k} = h\hat{x} + m\hat{z}$ is the wavenumber vector, h is the horizontal wavenumber, m is the vertical wavenumber, and $\underline{r} = x\hat{x} + z\hat{z}$ is the position vector. By assuming this same form for ζ, Gardner and Shelton (1985) derived the following closed-form solution for ζ, induced by a single gravity wave:

$$\zeta = \frac{g}{N^2} \ln\left(\frac{[M]}{\overline{[M]}}\right) = -\frac{g}{N^2} \ln\left(\frac{\theta}{\overline{\theta}}\right) + \frac{g}{N^2}\left(1 - \frac{R}{C_p}\right) \ln\left(\frac{p}{\overline{p}}\right). \tag{7}$$

Note that the right-hand side of (7) is derived by expressing $[M]$ in terms of the potential temperature ($\theta = T(p_0/p)^{R/C_p}$) and atmospheric pressure (p), where p_0 = 1,000 mb is the standard reference pressure, and R = 287 $\mathrm{m^2 \cdot K^{-1} \cdot s^{-2}}$ is the gas constant for dry air. We assume that the gravity wave perturbations of p and θ are small so that (7) may be linearized:

$$\zeta \simeq \frac{g}{N^2}\frac{[M]'}{\overline{[M]}} = -\frac{g}{N^2}\left(\frac{T'}{\overline{T}} - \frac{p'}{\overline{p}}\right) = -\frac{g}{N^2}\frac{\theta'}{\overline{\theta}} + \frac{g}{N^2}\left(1 - \frac{R}{C_p}\right)\frac{p'}{\overline{p}}. \tag{8}$$

If two or more gravity waves are present, then ζ will include the contributions of each individual wave given by (7), as well as contributions from the nonlinear interactions among the waves. These nonlinear interactions are second- and higher-order effects, which are proportional to the products of the wave amplitudes. Because we have assumed that the gravity wave perturbations are small enough to neglect the nonlinear contributions of θ' and p' to (7) so that ζ may be approximated by (8), we may also assume that in the presence of multiple waves, the second- and higher-order nonlinear interaction terms are also negligible. Therefore, the total vertical displacement associated with the full spectrum of waves is approximately equal to sum of the displacements associated with each individual wave, which are approximately linearly related to the sum of the individual temperature, pressure, and potential temperature fluctuations as shown by (8). Hence, the effective wave diffusivity is given by

$$K_{\mathrm{Wave}} \simeq \frac{g}{N^2}\frac{\overline{w'[M]'}}{\overline{[M]}} = K_H + \left(\frac{C_p}{R} - 1\right) K_E \ , \tag{9}$$

where

$$K_H = -\frac{g}{N^2}\frac{\overline{w'\theta'}}{\overline{\theta}} \ , \tag{10}$$

$$K_E = \frac{g}{N^2}\frac{R}{C_p}\frac{\overline{w'p'}}{\overline{p}} \ , \tag{11}$$

and

$$K_H - K_E = -\frac{g}{N^2}\frac{\overline{w'T'}}{\overline{T}} = \frac{-\overline{w'T'}}{\left(\Gamma_{\mathrm{ad}} + \partial\overline{T}/\partial z\right)}. \tag{12}$$

Note that to derive the right-hand side of (12), we used the definition for the square of the buoyancy frequency, namely, $N^2 = g\left(\Gamma_{\rm ad} + \partial\overline{T}/\partial z\right)/\overline{T}$. From (3), (9), and (12), we see that the total dynamical diffusivity $K_{\rm Dyn}$, associated with waves and turbulence, is given by

$$K_{\rm Dyn} = (1+\xi_{\rm inst})K_{zz} + K_{\rm Wave} = (1+\xi_{\rm inst})K_{zz} + \frac{C_p}{R}K_E - \frac{\overline{w'T'}}{\left(\Gamma_{\rm ad} + \partial\overline{T}/\partial z\right)} \tag{13}$$

where

$$\xi_{\rm inst} = \frac{\overline{\left(\partial T'/\partial z\right)^2}}{\left(\Gamma_{\rm ad} + \partial\overline{T}/\partial z\right)^2} \simeq \frac{\overline{\left(\partial u'/\partial z\right)^2}}{N^2} = \overline{1/Ri}. \tag{14}$$

The importance of $\xi_{\rm inst}$ will become apparent in the following section. This parameter is a measure of the instability of the atmosphere through which the waves are propagating. It is approximately equal to the mean of the inverse Richardson number *Ri*. In the mesopause region at SOR and CP, $\xi_{\rm inst}$ varies between about 0.1 and 0.6.

4. Parameterizing $K_{\rm Wave}$ and $K_{\rm Dyn}$

To incorporate wave transport into a global circulation model, it is necessary to compute the key transport parameters in equations (1)–(4) from data provided by the gravity wave, turbulence, and molecular diffusion modules incorporated within the model. For example, the Whole Atmosphere Community Climate Model (WACCM) employs a wave parameterization scheme that is based on a spectral model which includes waves excited in the atmosphere when stably stratified air flows over an irregular boundary and also by internal heating and shear (Beres et al., 2004, 2005; Garcia et al., 2007; Richter et al., 2010). WACCM computes the horizontal wind amplitudes, periods, and vertical wavelengths of the generated waves as a function of altitude, latitude, longitude, time of day, and season. As the waves propagate upward, the intervening wind and temperature fields, associated with the mean state of the atmosphere, modify the waves. The modifications include critical layer filtering and wave breaking. K_{zz} is computed when there is wave dissipation. Thus, WACCM can provide the wave spectrum and K_{zz} at each point in the model consistent with its resolution, as well as the mean atmospheric state (i.e., $\overline{T}$ and N^2). Obviously, the required variances of the wave-induced temperature and lapse rate fluctuations can be computed from the wave spectrum as can the wave energy flux $\overline{w'p'}$ and K_E (Gardner, 2018; Liu, 2009). The only parameters that cannot be computed from gravity wave data provided by WACCM and other global circulation models that employ similar wave parameterization schemes are the heat flux $\overline{w'T'}$ and K_H, which is proportional to the vertical flux of potential temperature $\overline{w'\theta'}$.

K_H is calculated following H-L. Liu (2000), who considered the impact of localized turbulence on a single gravity wave. In our case, we consider the combined effects of both turbulence and the full spectrum of waves and assume that the resulting diffusivity ($K_{\rm Dyn}$) is uniform. Because potential temperature is a conserved quantity, its fluctuations induced by gravity waves and turbulence are described by the continuity equation. Thus, the thermodynamic equation for heat flow in the presence of potential temperature gradients in an incompressible flow can be expressed as

$$\frac{\partial\theta}{\partial t} + \nabla\bullet\left(\underline{V}\theta - K_{\rm Dyn}\nabla\theta\right) = 0. \tag{15}$$

The linearized form of this equation, assuming the divergence of the mean wind field is zero, is given by

$$\frac{\partial\theta'}{\partial t} + \overline{u}\frac{\partial\theta'}{\partial x} + w'\frac{\partial\overline{\theta}}{\partial z} = \frac{\partial K_{\rm Dyn}}{\partial z}\frac{\partial\theta'}{\partial z} + K_{\rm Dyn}\frac{\partial^2\theta'}{\partial z^2}. \tag{16}$$

Note that (16) is identical to equation (1) in H-L. Liu (2000) for the special case of uniform $K_{\rm Dyn}$. By multiplying both sides of (16) by θ', taking the average and rearranging terms, we obtain

$$K_H = -\frac{g}{N^2}\frac{\overline{w'\theta'}}{\overline{\theta}} = K_{\mathrm{Dyn}}\frac{g^2}{N^4}\frac{\overline{\left(\partial\theta'/\partial z\right)^2}}{\overline{\theta}^2} \simeq \xi_{\mathrm{inst}} K_{\mathrm{Dyn}}. \tag{17}$$

The right-hand side of (17) is obtained by neglecting the small contribution of the pressure fluctuations to $\overline{\left(\partial\theta'/\partial z\right)^2}$. By combining (12), (13), and (17), we obtain these final results:

$$K_H \simeq \frac{\xi_{\mathrm{inst}}}{(1-\xi_{\mathrm{inst}})}\left[(1+\xi_{\mathrm{inst}})K_{zz} + \left(C_p/R-1\right)K_E\right] \tag{18}$$

$$K_{\mathrm{Dyn}} \simeq \frac{1}{(1-\xi_{\mathrm{inst}})}\left[(1+\xi_{\mathrm{inst}})K_{zz} + \left(C_p/R-1\right)K_E\right] \tag{19}$$

and

$$K_H - K_E \simeq \frac{1}{(1-\xi_{\mathrm{inst}})}\left[\xi_{\mathrm{inst}}(1+\xi_{\mathrm{inst}})K_{zz} + \left(\xi_{\mathrm{inst}}C_p/R-1\right)K_E\right]. \tag{20}$$

The total dynamical diffusivity associated with waves and turbulence, K_{Dyn} given by (19), can be computed from any gravity wave parameterization scheme that provides K_{zz} and the wave spectrum (or wave-driven T' and lapse rate variances), which are used to compute ξ_{inst} given by (14), K_E given by (11) and (21) (see below), and the chemical transport given by (4). K_{Dyn} is largest in regions where the atmospheric instability parameter ξ_{inst} is largest, which is expected to generally coincide with regions where K_{zz} is also largest.

5. Comparison With Observations

The efficacy of (18)–(20) can be assessed by comparing the predictions with extensive lidar measurements of wind, temperature, and heat flux profiles made in the mesopause region at the SOR, NM (34.96°N, 106.46°W; Gardner & Liu, 2007), and CP, Chile (30.25°S, 70.74°W; Guo et al., 2017). We focus on (12) and (20), which express K_H-K_E in terms of the measured heat flux or alternatively, in terms of K_{zz}, K_E, and ξ_{inst}. The data at both sites were acquired throughout the year (370 hr at SOR and 150 hr at CP). This complicates the comparison, because (20) involves a nonlinear combination of terms. However, we evaluate equation (20) using the mean values of those terms, ostensibly to achieve greater accuracy. Furthermore, K_{zz} was only measured at CP so a model K_{zz} profile was used for the SOR calculations. We do not believe these limitations are serious, because our goal is to confirm (20) predicts values of K_H-K_E that are in reasonable agreement with the values derived from the measured heat flux using (12).

We follow the approach suggested by Liu (2009) to compute K_E using a model for the joint vertical wavenumber and temporal frequency spectrum of the wave-induced temperature fluctuations, which yields (Gardner, 2018)

$$K_E = \frac{\gamma(1-2\alpha_{\mathrm{dwn}})\Gamma_{\mathrm{ad}}}{\overline{T}}\frac{\lambda_z^*}{\tau_i}\frac{\overline{\left(T'\right)^2}}{\left(\Gamma_{\mathrm{ad}}+\partial\overline{T}/\partial z\right)^2} \simeq \begin{cases} 0.426\overline{\left(T'\right)^2}\,\mathrm{m^2{\cdot}s^{-1}{\cdot}K^{-2}} \text{ at SOR} \\ 0.481\overline{\left(T'\right)^2}\,\mathrm{m^2{\cdot}s^{-1}{\cdot}K^{-2}} \text{ at CP} \end{cases}. \tag{21}$$

γ is a dimensionless parameter that depends on the shape of the temperature spectrum and data acquisition/processing parameters, α_{dwn} is the fraction of wave energy propagating downward (assumed to be 0.15), and τ_i is the inertial period. λ_z^* is the characteristic vertical wavenumber, which is computed from the ratio of the temperature and lapse rate variances using a suitable model for the vertical wavenumber spectrum of the temperature fluctuations. Most theories for the gravity wave vertical wavenumber (m) spectrum predict a power law dependence proportional to m^s for $0 \le m \le m_*$ and m^{-p} for $m_* \le m$, where $s \sim 1$ and $p \sim 3$ (Gardner, 1996). λ_z^* was derived using this spectral model with $s = 1$ and $p = 3$ along with the measured temperature and lapse rate variances. Where appropriate, certain parameters values were averaged over 85–100 km at each site and are tabulated in Table 1. Notice that K_E given by (21) and $\overline{w}_{\mathrm{Chem}}$ given by (4) are both proportional to $\overline{\left(T'\right)^2}/\left(\Gamma_{\mathrm{ad}}+\partial\overline{T}/\partial z\right)^2$. This parameter is approximately equal to $\overline{\zeta^2}$, the mean square displacement of the atmosphere induced by the full spectrum of waves. In the mesopause region at SOR and CP, the displacement parameter varies between about 0.6 and 1 $\mathrm{km^2}$.

Table 1
Mean Atmospheric Parameters (85–100 km) at SOR and CP

Parameter	SOR (34.96°N, 106.46°W)	CP (30.25°S, 70.74°W)
γ	4.56	4.87
$\partial\overline{T}/\partial z$	−0.488 K/km	−0.929 K/km
$\overline{T}$	192.7 K	188.4 K
$(\Gamma_{ad}+\partial\overline{T}/\partial z)^2$	80.7 K^2/km^2	73.0 K^2/km^2
λ_z^*	16.5 km	17.6 km
$\tau_i = 12\ h/\sin\phi_{Lat}$	20.9 hr	23.9 hr

Note. SOR = Starfire Optical Range; CP = Cerro Pachón.

The K_H-K_E profiles were derived at both sites from the measured heat flux according to (12) and also calculated using (20). The results for SOR and CP are plotted in Figures 1a and 1b, respectively. The parameters K_{zz}, K_E, and ξ_{inst} are plotted in Figure 2 for both sites. The K_{zz} model profile for SOR is a simple Gaussian distribution with a maximum value of 75 m^2/s at 88 km, where the measured heat flux peaks, and a root-mean-square width of 5 km. The uncertainty is conservatively estimated to be $\pm 20\ m^2/s$. Because of the shorter observation period at CP, to reduce the uncertainties, the CP data were smoothed using a running average of 3-km full width.

At both sites the measured and predicted K_H-K_E profiles are in reasonable agreement as the general shapes and values of the profiles are comparable. The profiles exhibit maximum values between 88 and 90 km of between 100 and 200 m^2/s. This corresponds to the altitude region where the instability parameter ξ_{inst} also reaches its maximum value. The K_H-K_E profiles then decrease with increasing altitude with the smallest values occurring between 97 and 99 km. Here, the measured profiles at both sites become negative with values varying between −10 and −30 m^2/s. However, only the predicted profile at SOR becomes negative. According to (20), negative values can only occur in regions of high atmospheric stability where $\xi_{inst} < R/C_p = 0.286$ and K_E is large compared to K_{zz}. In fact, in regions of very high atmospheric stability ($\xi_{inst} \sim 0$), wave dissipation is negligible so that $K_H = 0$. In this limiting case both (12) and (20) are equal to $-K_E$.

The uncertainty in the predicted K_H-K_E profile given by (20) is dominated by uncertainties in ξ_{inst} and K_{zz} at SOR and by uncertainties in ξ_{inst} at CP. The predicted profile at CP does not become negative at these higher altitudes because the atmosphere is apparently too unstable as characterized by ξ_{inst}. This region is at the edge of the thermosphere and so it is possible that we may have overestimated the value of ξ_{inst} by employing the mean environmental lapse rate from 85 to 100 km listed in Table 1, which is negative. For example, if the environmental lapse rate is actually 0 in this region rather than the 85- to 100-km mean (−0.929 K/km), then ξ_{inst} would decrease by about 20% and the predicted K_H-K_E profile would be in better agreement with the measurements. This could also explain the discrepancy between the measured and predicted K_H-K_E profiles

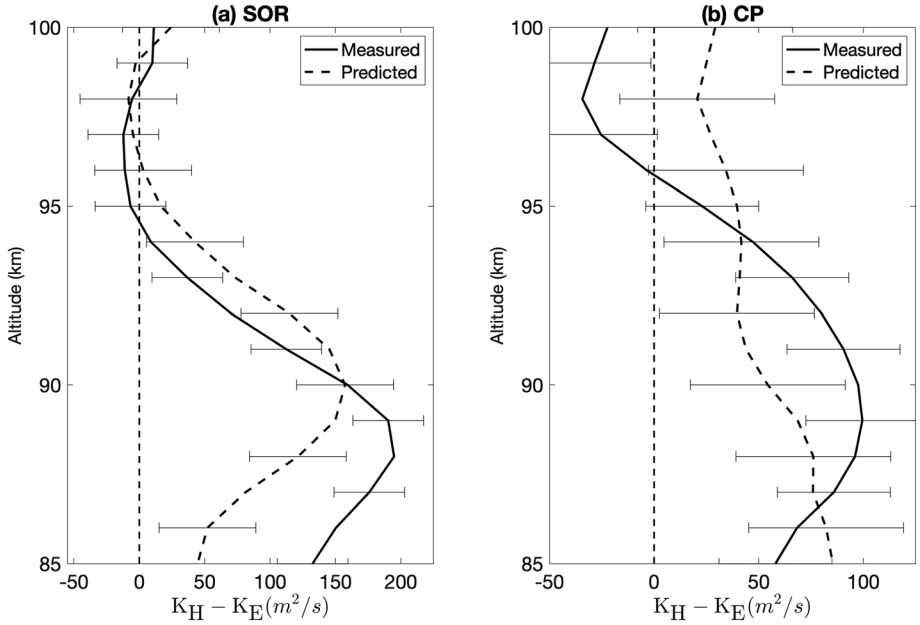

Figure 1. Profiles of K_H-K_E plotted between 85 and 100 km that were derived from the measured heat flux profile using equation (12) (solid curve) and that were predicted by equation (20) (dashed curve): (a) Starfire Optical Range, NM (34.96°N), and (b) Cerro Pachón, Chile (30.25°S).

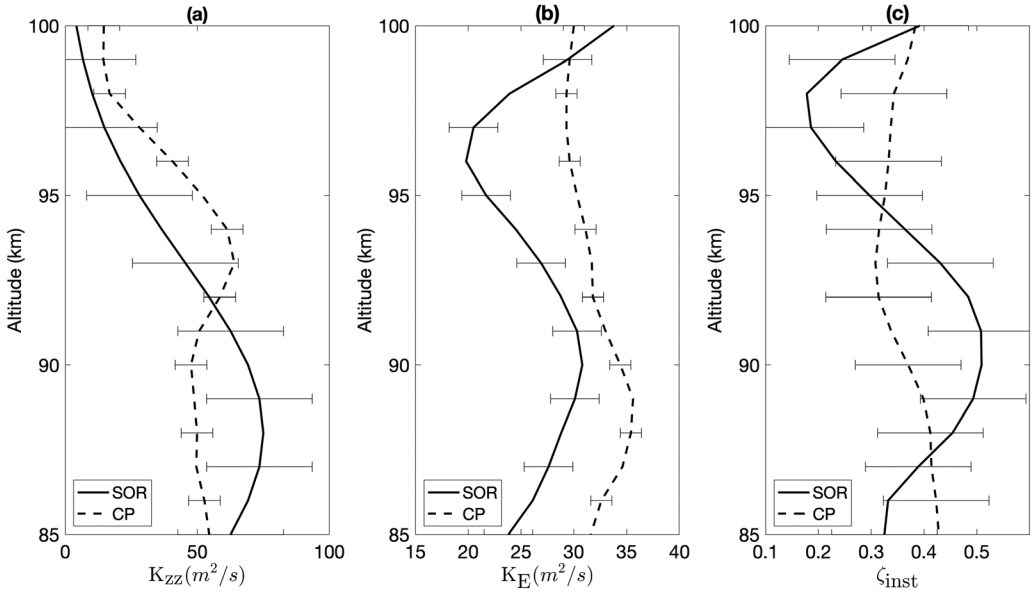

Figure 2. Profiles of the parameters: (a) eddy diffusivity K_{zz}, (b) diffusivity associated with wave energy flux K_E, and (c) instability parameter ζ_{inst}, all plotted between 85 and 100 km at the Starfire Optical Range (SOR), NM (34.96°N), (solid curve) and Cerro Pachón (CP), Chile (30.25°S), (dashed curve). The model K_{zz} profile at SOR is a Gaussian distribution with a maximum of 75 m^2/s at 88 km and a root-mean-square width of 5 km. The measured K_{zz} profile at CP is adapted from Guo et al. (2017).

at SOR at the lowest altitudes between 85 and 88 km. This region is just below the mesopause where observations and models predict negative lapse rates as high −1.5 to −2.0 K/km depending on the time of year. If the mean environmental lapse rate is −1.5 K/km in this region instead of −0.488 K/km that we computed for the 85- to 100-km mean, then ξ_{inst} would increase by about 27% and the predicted K_H-K_E profile would also

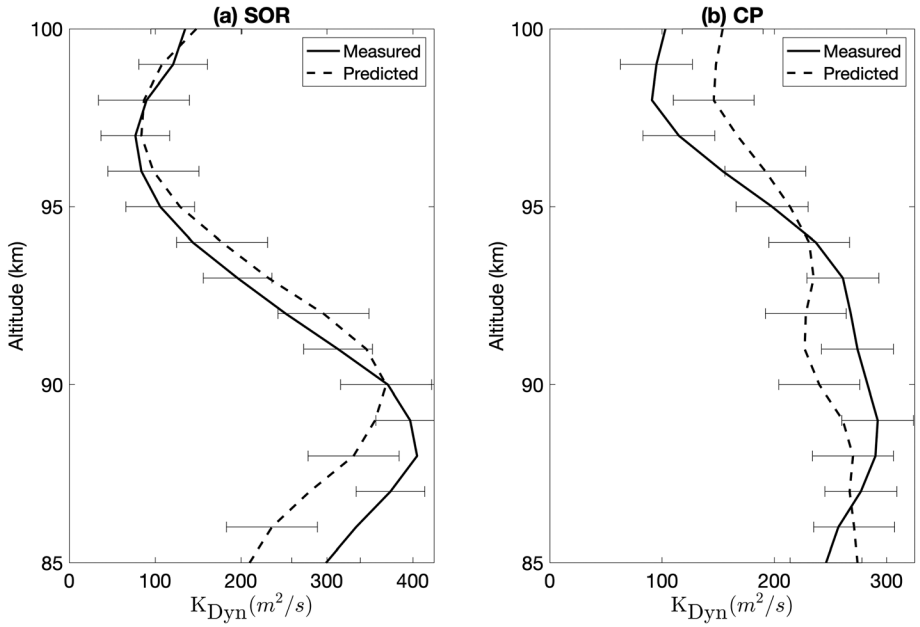

Figure 3. Profiles of K_{Dyn} plotted between 85 and 100 km that were derived from the measured heat flux profile using equation (13) (solid curve) and that were predicted by equation (19) (dashed curve): (a) Starfire Optical Range (SOR), NM (34.96°N) and (b) Cerro Pachón (CP), Chile (30.25°S). The mean and root-mean-square differences between the profiles (measured-predicted) are, respectfully, 13 and 50 m^2/s at SOR and −5.4 and 37 m^2/s at CP.

be in better agreement with the measurements. To improve accuracy when employing (19) and (20) in global models to estimate K_{Dyn} and K_H-K_E, the parameters ξ_{inst}, K_{zz}, and K_E, should be derived over short time intervals of about one month or less, instead using the annual mean values as we have done here.

Finally, the total dynamical diffusivity (K_{Dyn}) profiles were calculated using (13) and the measured heat flux profiles and predicted by (19) using ξ_{inst}, K_{zz}, and K_E. The results are plotted for comparison in Figure 3a for SOR and Figure 3b for CP. The predicted K_{Dyn} profiles are in good agreement with the profiles computed from the measured heat flux, which means that (19) can be used to estimate the total dynamical diffusivity. Thus, existing global atmospheric models can now be modified to fully account for wave-induced constituent transport by replacing K_{zz} with K_{Dyn} calculated according to (19) and including the chemical transport described by (4). Notice that K_{Dyn} at both sites is many times larger than K_{zz} plotted in Figure 2a. The impact of the larger K_{Dyn} is expected to be significant, at least in the mesopause region, where measurements have shown that the modeled transport of meteoric Na and Fe is much weaker than observations and insufficient to accommodate the estimated meteoric influxes of these metals (Carrillo-Sánchez et al., 2016; Feng et al., 2013; Gardner et al., 2016; Marsh et al., 2013). Notice also that when there is no wave dissipation K_H, K_{zz}, and ξ_{inst} are 0 so that (9), (13), and (19) reduce to $K_{\mathrm{Wave}} = K_{\mathrm{Dyn}} = (C_p/R - 1)K_E$. In this limiting case, the random vertical displacements imparted by the full spectrum of nondissipating waves, still contribute to mixing of the atmosphere, which is characterized by a baseline diffusivity that is proportional to the wave energy flux, although it is small for most Boussinesq waves.

6. Conclusions

We have presented a solution for the effective wave diffusivity K_{Wave}, which accounts for the wave-driven vertical constituent transport that is currently missing in the gravity wave parameterizations employed in most general circulation models. The solution depends only on the eddy diffusion coefficient and variances of the temperature and lapse rate fluctuations, which are readily available from contemporary wave parameterization schemes. Therefore, it is now feasible to include a physically consistent representation of constituent transport effects in global circulation models. However, if implemented, it is likely the altered model simulations will deviate from their current "correct" state, which will have to be compensated by tuning other parameters. Thus, this improved representation of gravity wave transport will also help constrain the tuning of key model parameters.

The solution for K_{Wave} derived here is based upon an exact solution to (6) for monochromatic gravity waves (Gardner & Shelton, 1985). K_{Wave} is $(C_p/R)K_E \sim 100$ m^2/s larger than the solution derived by Gardner (2018), who used the first-order perturbation solution to (6). It is not difficult to show, that if the perturbation solution is employed in the section 4 analysis, then the predicted K_H-K_E profiles are in very poor agreement with those computed from the measured heat fluxes at both SOR and CP. Because chemistry is influenced primarily by temperature fluctuations, this new solution to (6) and for K_{Wave} has only a minor impact on chemical transport. In fact, when the production of the species is slow compared to the periods of the dominant gravity waves, the chemical transport of C is identical to that derived by Gardner (2018) and given by (4).

Although the comparison of theory with observations was focused on the mesopause region, the analysis is general and can be used to estimate wave transport at any altitude. All that is required is knowledge of the mean thermal state of the background atmosphere ($\overline{T}$), the temperature and lapse rate fluctuation variances induced by gravity waves ($\overline{\left(T'\right)^2}$ and $\overline{\left(\partial T'/\partial z\right)^2}$), and the eddy diffusivity (K_{zz}). The remaining parameters required to compute K_{Wave}, K_{Dyn}, and $\overline{w}_{\mathrm{Chem}}$ can be calculated from these four quantities. Thus, the results derived in this paper can also be used to assess the significance of wave-driven constituent transport throughout the atmosphere. For example, in the lower thermosphere, the atmosphere is inherently more stable because the environmental lapse rate is large and positive, but extensive rocket and lidar measurements have shown that wave amplitudes and wind shears are exceptionally large in the 100- to 110-km altitude range (Larsen, 2002; Yue et al., 2010). So even though turbulence is negligible in this region, the wave energy flux (and K_E) and the instability parameter ξ_{inst} can be large so that K_{Dyn} could become comparable to or even greater than the molecular diffusivity. Similarly, in the middle and lower mesosphere the mean lapse rate is negative so the atmosphere is less stable. When wave amplitudes become large enough to generate turbulence in this region through wave breaking, ξ_{inst}, K_{zz}, and K_E could also be large enough to induce

significant enhancements in K_{Dyn}. Balloon, lidar, and radar observations of temperatures, winds, and turbulence, made throughout the atmosphere, in combination with the expressions derived here, can now be used to assess the significance of wave transport at all altitudes and to model its effects.

Acknowledgments
The data used in this work are tabulated in the supporting information to this paper. This work was supported in part by National Science Foundation grants OPP 12-46431, AGS-1734553, and AGS-1759471.

References

Beres, J. H., Alexander, M. J., & Holton, J. R. (2004). A method of specifying the gravity wave spectrum above convection based on latent heating properties and background wind. *Journal of the Atmospheric Sciences*, *61*, 324–337.

Beres, J. H., Garcia, R. R., Boville, B. A., & Sassi, F. (2005). Implementation of a gravity wave source spectrum parameterization dependent on the properties of convection in the Whole Atmosphere Community Climate Model (WACCM). *Journal of Geophysical Research*, *110*, D10108. https://doi.org/10.1029/2004JD005504

Carrillo-Sánchez, J. D., Nesvorn, D., Pokorny, P., Janches, D., & Plane, J. M. C. (2016). Sources of cosmic dust in the Earth's atmosphere. *Geophysical Research Letters*, *43*, 11,979–11,986. https://doi.org/10.1002/2016GL071697

Coy, L., Fritts, D. C., & Weinstock, J. (1986). The Stokes drift due to vertically propagating internal gravity waves in a compressible atmosphere. *Journal of the Atmospheric Sciences*, *43*(22), 2636–2643. https://doi.org/10.1175/1520-0469(1986)043<2636:TSDDTV>2.0.CO;2

Crutzen, P. J. (1970). The influence of nitrogen oxides on the atmospheric ozone content. *Quarterly Journal of the Royal Meteorological Society*, *96*, 320–325.

Feng, W., Marsh, D. R., Chipperfield, M. P., Janches, D., Höffner, J., Yi, F., & Plane, J. M. C. (2013). A global atmospheric model of meteoric iron. *Journal of Geophysical Research: Atmospheres*, *118*, 9456–9474. https://doi.org/10.1002/jgrd.50708

Garcia, R. R., Lopez-Puertas, M., Funke, B., Marsh, D. R., Kinnison, D. E., & Smith, A. K. (2014). On the distribution of CO_2 and CO in the mesosphere and thermosphere. *Journal of Geophysical Research: Atmospheres*, *119*, 5700–5718. https://doi.org/10.1002/2013JD021208

Garcia, R. R., Marsh, D. R., Kinnison, D. E., Boville, B. A., & Sassi, F. (2007). Simulation of secular trends in the middle atmosphere, 1950–2003. *Journal of Geophysical Research*, *112*, D09301. https://doi.org/10.1029/2006JD007485

Garcia, R. R., & Solomon, S. (1985). The effects of breaking gravity waves on the dynamics and chemical composition of the mesosphere and lower thermosphere. *Journal of Geophysical Research*, *90*, 3850–3868. https://doi.org/10.1029/JD090iD02p03850

Garcia, R. R., & Solomon, S. (1994). A new numerical model of the middle atmosphere. 2. Ozone and related species. *Journal of Geophysical Research*, *99*(D6), 12,937–12,952. https://doi.org/10.1029/94JD00725

Gardner, C. S. (1996). Testing theories of atmospheric gravity wave saturation and dissipation. *Journal of Atmospheric and Terrestrial Physics*, *58*(14), 1575–1589. https://doi.org/10.1016/0021-9169(96)00027-X

Gardner, C. S. (2018). Role of wave-induced diffusion and energy flux in the vertical transport of atmospheric constituents in the mesopause region. *Journal of Geophysical Research: Atmospheres*, *123*, 6581–6604. https://doi.org/10.1029/2018JD028359

Gardner, C. S., & Liu, A. Z. (2007). Seasonal variations of the vertical fluxes of heat and horizontal momentum in the mesopause region at Starfire Optical Range, New Mexico. *Journal of Geophysical Research*, *112*, D09113. https://doi.org/10.1029/2005JD006179

Gardner, C. S., & Liu, A. Z. (2010). Wave-induced transport of atmospheric constituents and its effect on the mesospheric Na layer. *Journal of Geophysical Research*, *115*, D20302. https://doi.org/10.1029/2010JD014140

Gardner, C. S., & Liu, A. Z. (2016). Chemical transport of neutral atmospheric constituents by waves and turbulence: Theory and observations. *Journal of Geophysical Research: Atmospheres*, *121*, 494–520. https://doi.org/10.1002/2015JD023145

Gardner, C. S., Liu, A. Z., & Guo, Y. (2016). Vertical and horizontal transport of mesospheric Na: Implications for the mass influx of cosmic dust. *Journal of Atmospheric and Solar - Terrestrial Physics*. https://doi.org/10.1016/j.jastp.2016.07.013

Gardner, C. S., & Shelton, J. D. (1985). Density response of neutral atmospheric layers to gravity wave perturbations. *Journal of Geophysical Research*, *90*(A2), 1745–1754. https://doi.org/10.1029/JA090iA02p01745

Grygalashvyly, M., Becker, E., & Sonnemann, G. R. (2012). Gravity wave mixing and effective diffusivity for minor chemical constituents in the mesosphere/lower thermosphere. *Space Science Reviews*, *168*, 333–362. https://doi.org/10.1007/s11214-011-9857-x

Guo, Y., Liu, A. Z., & Gardner, C. S. (2017). First Na lidar measurements of turbulence heat flux, thermal diffusivity and energy dissipation rate in the mesopause region. *Geophysical Research Letters*, *44*, 5782–5790. https://doi.org/10.1002/2017GL073807

Larsen, M. F. (2002). Winds and shears in the mesosphere and lower thermosphere: Results from four decades of chemical release wind measurements. *Journal of Geophysical Research*, *107*(A8), 1215. https://doi.org/10.1029/2001JA000218

Lary, D. J. (1997). Catalytic destruction of stratospheric ozone. *Journal of Geophysical Research*, *102*, 21,515–21,526. https://doi.org/10.1029/97JD00912

Liu, A. Z. (2009). Estimate eddy diffusion coefficients from gravity wave vertical momentum and heat fluxes. *Geophysical Research Letters*, *36*, L08806. https://doi.org/10.1029/2009GL037495

Liu, A. Z., & Gardner, C. S. (2004). Vertical dynamical transport of mesospheric constituents by dissipating gravity waves. *Journal of Atmospheric and Solar - Terrestrial Physics*, *66*(3-4), 267–275. https://doi.org/10.1016/j.jastp.2003.1011.1002

Liu, H.-L. (2000). Temperature changes due to gravity wave saturation. *Journal of Geophysical Research*, *105*(D10), 12,329–12,336. https://doi.org/10.1029/2000JD900054

Marsh, D. R., Garcia, R. R., Kinnison, D. E., Boville, B. A., Sassi, F., Solomon, S. C., & Matthes, K. (2007). Modeling the whole atmosphere response to solar cycle changes in radiative and geomagnetic forcing. *Journal of Geophysical Research*, *112*, D23306. https://doi.org/10.1029/2006JD008306

Marsh, D. R., Janches, D., Feng, W., & Plane, J. M. C. (2013). A global model of meteoric sodium. *Journal of Geophysical Research: Atmospheres*, *118*, 11,442–11,452. https://doi.org/10.1002/jgrd.50870

Nakamura, N. (2001). A new look at eddy diffusivity as a mixing diagnostic. *Journal of the Atmospheric Sciences*, *58*(24), 3685–3701. https://doi.org/10.1175/1520-0469(2001)

Plane, J. M. C. (2012). Cosmic dust in the Earth's atmosphere. *Chemical Society Reviews*, *41*(19), 6507–6518. https://doi.org/10.1039/C2CS35132C

Plane, J. M. C., Feng, W., & Dawkins, E. C. M. (2015). The mesosphere and metals: Chemistry and changes. *Chemical Reviews*, *115*(10), 4497–4541. https://doi.org/10.1021/cr50051m

Richter, J. H., Sassi, F., & Garcia, R. R. (2010). Towards a physically based gravity wave source parameterization in a general circulation model. *Journal of the Atmospheric Sciences*, *67*, 136–156.

Shepherd, G. G., Liu, G., & Roble, R. G. (2004). Remote sensing of the large-scale circulation of atomic oxygen. In K. Schafer, A. Comeron, M. R. Carleer, R. H. Picard, & N. I. Sifakis (Eds.), *Remote Sensing of Clouds and the Atmosphere IX*, *Proceedings of SPIE* (Vol. 5571, pp. 173–181). Maspalomas, Canary Islands, Spain. Retrieved from www.spiedigitallibrary.org/conference-proceedingsof-SPIE/5571

Smith, A. K., Marsh, D. R., Mlynczak, M. G., & Mast, J. C. (2010). Temporal variations of atomic oxygen in the upper atmosphere from SABER. *Journal of Geophysical Research*, *115*, D18309. https://doi.org/10.1029/2009JD013434

Walterscheid, R. L. (1981). Dynamical cooling induced by dissipating internal gravity waves. *Geophysical Research Letters*, *8*(11), 1235–1238. https://doi.org/10.1029/GL008i012p01235

Walterscheid, R. L., & Schubert, G. (1989). Gravity-wave fluxes of O_3 and OH at the nightside mesopause. *Geophysical Research Letters*, *16*(7), 719–722.

Ward, W. E. (1999). A simple model of diurnal variations in the mesospheric oxygen nightglow. *Geophysical Research Letters*, *26*(23), 3565–3568. https://doi.org/10.1029/1999GL003661

Winters, K. B., & D'Asaro, E. A. (1996). Diascalar flux and the rate of fluid mixing. *Journal of Fluid Mechanics*, *317*, 179–193. https://doi.org/10.1017/S0022112096000717

Xu, J., Smith, A. K., & Ma, R. (2003). A numerical study of the effect of gravity wave propagation on minor species distributions in the mesopause region. *Journal of Geophysical Research*, *108*(D3), 4119. https://doi.org/10.1029/2001JD001570

Yue, J., She, C.-Y., & Liu, H.-L. (2010). Large wind shears and stabilities in the mesopause region observed by Na wind-temperature lidar at midlatitude. *Journal of Geophysical Research*, *115*, A10307. https://doi.org/10.1029/2009JA014864

Zhu, X., Yee, J. H., Swartz, W. H., & Talaat, E. R. (2010). A spectral parameterization of drag, eddy diffusion, and wave heating for a three-dimensional flow induced by breaking gravity waves. *Journal of the Atmospheric Sciences*, *67*, 2520–2536. https://doi.org/10.1175/2010JAS3302.1